Advances in Materials Research, *Vol. 10*, *No. 4* (*2021*) *293-311*
https://doi.org/10.12989/amr.2021.10.4.293

Effect of porosity on the free vibration analysis of various functionally graded sandwich plates

Mohamed Saad [1,2], Lazreg Hadji*[1,3] and Abdelouahed Tounsi [4,5,6]

[1] *Department of Mechanical Engineering*, *University of Tiaret*, *BP 78 Zaaroura*, *14000 Tiaret*, *Algeria*
[2] *Laboratory of Industrial Technology*, *Department of Mechanical Engineering*, *University of Tiaret*, *Algeria*
[3] *Laboratory of Geomatics and Sustainable Development*, *Ibn Khaldoun University of Tiaret*, *Algeria*
[4] *Material and Hydrology Laboratory*, *Faculty of Technology*, *Civil Engineering Department*, *University of Sidi Bel Abbes*, *Algeria*
[5] *YFL* (*Yonsei Frontier Lab*), *Yonsei University*, *Seoul*, *Korea*
[6] *Department of Civil and Environmental Engineering*, *King Fahd University of Petroleum & Minerals*, *31261 Dhahran*, *Eastern Province*, *Saudi Arabia*

(*Received November 24*, *2020*, *Revised September 6*, *2021*, *Accepted September 19*, *2021*)

Abstract. In this paper, a simple refined shear deformation theory which eliminates the use of a shear correction factor was presented for free vibration analysis of FG sandwich plates composed of FG porous face sheets and an isotropic homogeneous core. Unlike any other theory, the number of unknown functions involved is only four, as against five in case of other shear deformation theories. Material properties of FGM layers are assumed to vary continuously across the plate thickness according to either power-law function in terms of the volume fractions of the constituents. The face layers are considered to be FG porous across each face thickness while the core is made of a ceramic homogeneous layer. Four models of porosity distribution are proposed. Governing equations and boundary conditions are derived from Hamilton's principle. Analytical solutions were obtained for free vibration analysis of square sandwich plates with FG porous layers under various boundary conditions. Numerical results are presented to show the effect of the porosity volume fraction, type of porosity distribution model, side to thickness ratio, lay-up scheme, and boundary conditions on the free vibration of FG sandwich plates. The validity of the present theory is investigated by comparing some of the present results with other published results.

Keywords: free vibration; functionally graded materials; porosity; power-law function; sandwich plates

1. Introduction

In recent years, functionally graded materials (FGMs) in which the volume fractions of material constituents vary gradually along certain direction have received great attention in many engineering applications (i.e., space vehicles, aircrafts, electronics, shipbuilding, biomedical applications and defense industries) owing to their superior mechanical and thermal properties. These new materials were proposed by material scientists in Japan in 1984 to eliminate interface problems and stress concentrations. With the developments in manufacturing methods, the FGMs are considered in the industry of the sandwich structures because of the gradual variation of

*Corresponding author, Ph.D., E-mail: had_laz@yahoo.fr

 ISSN: 2234-0912 (Print), 2234-179X (Online)

material properties at the interfaces between the face layers and the core. The key limitation in using FG sandwich structures in traditional industries is because of the high cost of production of this material.

Because of the importance and applications of the FGM sandwich structures, understanding of their responses becomes an important task. Several researches have been performed to analyzed the free vibration behavior of FG sandwich plates.

Zenkour (2005) presented a comprehensive analysis of functionally graded sandwich plates: Part 2—Buckling and free vibration. Ebrahimi and Salari (2016) studied thermal loading effects on electro-mechanical vibration behavior of piezoelectrically actuated inhomogeneous size-dependent Timoshenko nanobeams. Ebrahimi and Salari (2017) developed semi-analytical vibration analysis of functionally graded size-dependent nanobeams with various boundary conditions. Ashoori *et al*. (2017) developed size-dependent axisymmetric vibration of functionally graded circular plates in bifurcation/limit point instability.

In last years, many researchers interested in investigation of porous functionally graded materials; Wattanasakulpong and Ungbhakorn (2014) studied vibration characteristics of FGM porous beams by using differential transformation method with different kinds of elastic supports. Wang *et al*. (2014) developed a new suggestion for determining 2D porosities in DEM studies. Ebrahimi and Jafari (2016) investigated thermal vibration of FGM porous beams. Zouatnia *et al*. (2017) developed an analytical solution for bending and vibration responses of functionally graded beams with porosities. Akbaş (2017) examined the vibration and static analysis of functionally graded plates with porosity. Ebrahimi and Salari (2017) analyze the thermo-mechanical vibration of functionally graded micro/nanoscale beams with porosities based on modified couple stress theory. Ahmadi (2017) used a Galerkin Layerwise formulation for three-dimensional stress analysis in long sandwich plates. Wu *et al*. (2018) performed a finite element analysis to study the free and forced vibration FGM porous beam using both Euler-Bernoulli and Timoshenko beam theories. Yang *et al*. (2018) used Chebyshev-Ritz method to study buckling and free vibration of FGM graphene reinforced porous nanocomposite. Taati and Fallah (2019) presented forced vibration of sandwich modified strain gradient microbeams with FGM core. Salari *et al*. (2019) investigated the porosity-dependent asymmetric thermal buckling of inhomogeneous annular nanoplates resting on elastic substrate. Avcar (2019) investigated the free vibration of imperfect sigmoid and power law functionally graded beams. Salari *et al*. (2020) studied nonlinear thermal behavior of shear deformable FG porous nanobeams with geometrical imperfection: Snap-through and postbuckling analysis. Salari and Vanini (2021) investigated of thermal preloading and porosity effects on the nonlocal nonlinear instability of FG nanobeams with geometrical imperfection. Cuong-Le *et al*. (2021) used a three-dimensional solution for free vibration and buckling of annular plate, conical, cylinder and cylindrical shell of FG porous-cellular materials using IGA.

Since complex fabrication processes of the FGMs, micro voids and porosities often occur. During these procedures, due to the large difference in the solidification temperature of the FGM material constituents a certain number of defects appears. Then, we can say that the porosities are related with the distribution of the FGM material constituents. For these reasons, we present in this study, a new porosities distribution for free vibration analysis of new model of functionally graded material (FGM) sandwich plates. Material properties of FGM layers are assumed to vary continuously across the plate thickness according to either power-law function in terms of the volume fractions of the constituents. The four-variable refined plate theory is proposed to derive the field equations of the FG sandwich plates under various boundary conditions. The most

interesting feature of this theory is that it does not require the shear correction factor and satisfies equilibrium conditions at the top and bottom faces of the sandwich plate. Governing equations and boundary conditions are derived from Hamilton's principle. Analytical solutions were obtained for free vibration analysis of square sandwich plates with FG porous layers under various boundary conditions. Numerical examples are presented to verify the accuracy of the present theory. Numerical results are presented to show the effect of the material distribution, the sandwich plate geometry and the porosity on the free vibration of FG sandwich plates.

2. FGM sandwich plates

Consider the case of a uniform thickness, rectangular FGM sandwich plate composed of three microscopically heterogeneous layers, with reference to rectangular coordinates (x, y, z) as depicted in Fig. 1. The upper and lower faces of the plate are at $z = \pm h/2$, and the edges of the plate are parallel to the x and y axes.

The sandwich plate is composed of three elastic layers, namely "Layer 1," "Layer 2," and "Layer 3" from the uppermost surface to the lowest surface of the plate. The vertical coordinates of the base, the two interfaces, and the top are denoted by $h_0 = -h/2$, h_1, h_2, and $h_3 = +h/2$, respectively.

For brevity, the ratio of the thickness of each layer from the base to the top is denoted by the combination of three numbers, i.e., "1–0–1," "2–1–2," and so on.

The face layers of the sandwich plate are synthesized of an isotropic material with material properties varying smoothly in the z (thickness) direction only. The core layer is made of an isotropic homogeneous material as again illustrated in Fig. 1. The properties of P-FGM vary continuously due to gradually changing the volume fraction of the constituent materials, generally in the thickness direction only. The volume fraction of the sandwich plate faces varies according to a simple power law function of z while that of the core equals unity, and they are given as

$$V^{(1)}(z) = \left(\frac{z - h_0}{h_1 - h_0}\right), \qquad h_0 \le z \le h_1 \tag{1a}$$

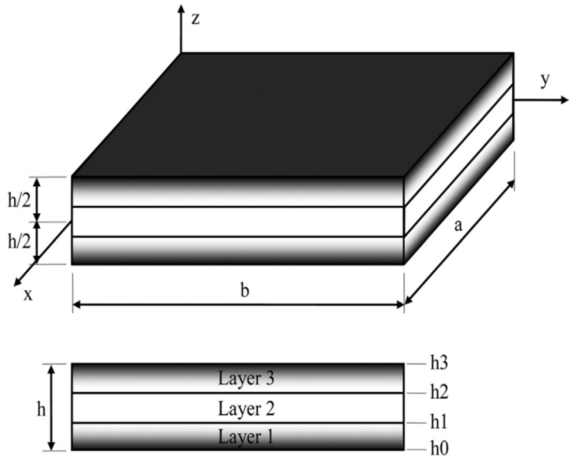

Fig. 1 Geometry and coordinates of FG sandwich plates

$$V^{(2)}(z) = 1, \qquad h_1 \le z \le h_2 \tag{1b}$$

$$V^{(3)}(z) = \left(\frac{z - h_3}{h_2 - h_3}\right), \qquad h_2 \le z \le h_3 \tag{1c}$$

Where k denotes volume fraction index. When $k = 0$ we return to the fully homogeneous ceramic plate.

3. Porosity-dependent FG sandwich plates

Effective material properties of FGMs are influenced by various factors such as high temperature, humidity and porosity. In this paper, the porosity effect is investigated. Numerous models of porosities distribution have been proposed by the researchers to compute the effective material properties of porous FGM plate (Wattanasakulpong and Ungbhakorn 2014, Shahsavari *et al*. 2018, Gupta and Talha 2018). In this paper, for the first time, the porosities are distributed independently in each FGM layer of sandwich. Four models of porosity are used.

3.1 Imperfect FGM with even porosities (*Imperfect I*)

Let us assume that the FG sandwich plate is fabricated of a mixture of metal and ceramic. The influence of porosities, which may exist inside the materials of FGM layers during the production, is included. The porosities uniformly distributed over the FGM sandwich layers, whereas the core layer is perfect (nonporous) and made of ceramic. By using the rule of mixture, the effective material properties $P^{(n)}$ of layer n $(n = 1, 2, 3)$ with evenly distributed porosities (imperfect I), are stated as (Daikh and Zenkour 2019)

$$\begin{aligned} P^{(1)}(z) &= (P_c - P_m)V^{(1)}(z) + P_m - \frac{\alpha}{2}(P_c + P_m) \\ P^{(2)}(z) &= (P_c - P_m)V^{(2)}(z) + P_m \\ P^{(3)}(z) &= (P_c - P_m)V^{(3)}(z) + P_m - \frac{\alpha}{2}(P_c + P_m) \end{aligned} \tag{2}$$

where α denotes the porosity coefficient $(\alpha \prec\prec 1)$. P_c and P_m are the corresponding properties of the ceramic and metal, respectively.

3.2 Imperfect FGM with uneven porosities (*Imperfect II*)

Here, the porosities may spread functionally during the thickness direction of the FGM sandwich as follow (Daikh and Zenkour 2019)

$$\begin{aligned} P^{(1)}(z) &= (P_c - P_m)V^{(1)}(z) + P_m - \frac{\alpha}{2}(P_c + P_m)\left[1 - \frac{|2z - h_0 - h_1|}{h_1 - h_0}\right] \\ P^{(2)}(z) &= (P_c - P_m)V^{(2)}(z) + P_m \\ P^{(3)}(z) &= (P_c - P_m)V^{(3)}(z) + P_m - \frac{\alpha}{2}(P_c + P_m)\left[1 - \frac{|2z - h_3 - h_2|}{h_3 - h_2}\right] \end{aligned} \tag{3}$$

3.3 Imperfect FGM with logarithmic-uneven porosities (*Imperfect III*)

Another uneven model based on a logarithmic function can be expressed as (Daikh and Zenkour 2019)

$$\begin{aligned} P^{(1)}(z) &= (P_c - P_m)V^{(1)}(z) + P_m - log\left(1+\frac{\alpha}{2}\right)(P_c + P_m)\left[1 - \frac{|2z - h_0 - h_1|}{h_1 - h_0}\right] \\ P^{(2)}(z) &= (P_c - P_m)V^{(2)}(z) + P_m \\ P^{(3)}(z) &= (P_c - P_m)V^{(3)}(z) + P_m - log\left(1+\frac{\alpha}{2}\right)(P_c + P_m)\left[1 - \frac{|2z - h_3 - h_2|}{h_3 - h_2}\right] \end{aligned} \tag{4}$$

3.4 Imperfect FGM with linear-uneven porosities (*Imperfect IV*)

The density of porosity is low at the outer surfaces of the sandwich and high at the two interfaces positions, and change across the FGM layers with linear function as (Daikh and Zenkour 2019)

$$\begin{aligned} P^{(1)}(z) &= (P_c - P_m)V^{(1)}(z) + P_m - \frac{\alpha}{2}(P_c + P_m)\left[1 - \frac{z - h_1}{h_0 - h_1}\right] \\ P^{(2)}(z) &= (P_c - P_m)V^{(2)}(z) + P_m \\ P^{(3)}(z) &= (P_c - P_m)V^{(3)}(z) + P_m - \frac{\alpha}{2}(P_c + P_m)\left[\frac{z - h_3}{h_2 - h_3}\right] \end{aligned} \tag{5}$$

4. Mathematical formulation

4.1 Kinematics and constitutive equations

The displacement field of the present refined theory is given by

$$\begin{aligned} u(x,y,z) &= u_0(x,y,t) - z\frac{\partial w_b}{\partial x} - f(z)\frac{\partial w_s}{\partial x} \\ v(x,y,z) &= v_0(x,y,t) - z\frac{\partial w_b}{\partial y} - f(z)\frac{\partial w_s}{\partial y} \\ w(x,y,z) &= w_b(x,y) + w_s(x,y) \end{aligned} \tag{6}$$

Where u_0, v_0 denote the displacements along the x and y coordinate directions of a point on the mid-plane of the plate. w_b and w_s are the bending and shear components of the transverse displacement, respectively. It is clear that the displacement field in Eq. (6) contains only four unknowns (u_0, v_0, w_b, w_s). The shape function $f(z)$ is chosen to satisfy the stress-free boundary conditions on the top and bottom surfaces of the plate, thus a shear correction factor is not required. In this study, the shape function is considered

$$f(z) = z\left[-\frac{1}{4} + \frac{5}{3}\left(\frac{z}{h}\right)^2\right], \tag{7}$$

The strains associated with the displacements in Eq. (6) are

$$\begin{aligned}
&\varepsilon_x = \varepsilon_x^0 + z\, k_x^b + f(z)\, k_x^s \\
&\varepsilon_y = \varepsilon_y^0 + z\, k_y^b + f(z)\, k_y^s \\
&\gamma_{yz} = g(z)\, \gamma_{yz}^s \\
&\gamma_{xz} = g(z)\, \gamma_{xz}^s \\
&\varepsilon_z = 0
\end{aligned} \tag{8}$$

where

$$\begin{aligned}
&\varepsilon_x^0 = \frac{\partial u_0}{\partial x}, \qquad k_x^b = -\frac{\partial^2 w_b}{\partial x^2}, \qquad k_x^s = -\frac{\partial^2 w_s}{\partial x^2}, \\
&\varepsilon_y^0 = \frac{\partial v_0}{\partial x}, \qquad k_y^b = -\frac{\partial^2 w_b}{\partial y^2}, \qquad k_y^s = -\frac{\partial^2 w_s}{\partial y^2}, \\
&\gamma_{yz}^s = \frac{\partial w_s}{\partial x}, \qquad \gamma_{xz}^s = \frac{\partial w_s}{\partial x}, \qquad g(z) = 1 - f'(z), \qquad f'(z) = \frac{df(z)}{dz}
\end{aligned} \tag{9}$$

For elastic and isotropic FGMs, the constitutive relations can be written as

$$\begin{Bmatrix} \sigma_x \\ \sigma_y \\ \tau_{yz} \\ \tau_{xz} \\ \tau_{xy} \end{Bmatrix}^{(n)} = \begin{bmatrix} C_{11} & C_{12} & 0 & 0 & 0 \\ C_{12} & C_{22} & 0 & 0 & 0 \\ 0 & 0 & C_{44} & 0 & 0 \\ 0 & 0 & 0 & C_{55} & 0 \\ 0 & 0 & 0 & 0 & C_{66} \end{bmatrix}^{(n)} \begin{Bmatrix} \varepsilon_x \\ \varepsilon_y \\ \gamma_{yz} \\ \gamma_{xz} \\ \gamma_{xy} \end{Bmatrix}^{(n)} \tag{10}$$

where

$$C_{11}(z) = \frac{E(z)}{(1-v^2)}, \qquad C_{12}(z) = vC_{11}(z) \tag{11}$$

and

$$C_{44}(z) = C_{55}(z) = C_{66}(z) = \frac{E(z)}{2(1+v)} \tag{12}$$

4.3 Governing equations

Hamilton's principle is used herein to derive equations of motion. The principle can be stated in an analytical form as (Delale and Erdogan 1983)

$$\int_0^t (\delta U - \delta T) = 0 \tag{13}$$

where δU is the variation of strain energy and δT is the variation of kinetic energy. The variation of strain energy of the plate is calculated by

$$\begin{aligned}
\delta U &= \int_V \left[\sigma_x \delta \varepsilon_x + \sigma_y \delta \varepsilon_y + \tau_{xy} \delta \gamma_{xy} + \tau_{yz} \delta \gamma_{yz} + \tau_{xz} \delta \gamma_{xz}\right] dV \\
&= \int_A \left[N_x \delta \varepsilon_x^0 + N_y \delta \varepsilon_y^0 + N_{xy} \delta \gamma_{xy}^0 + M_x^b \delta k_x^b + M_y^b \delta k_y^b + M_{xy}^b \delta k_{xy}^b \right. \\
&\quad \left. + M_x^s \delta k_x^s + M_y^s \delta k_y^s + M_{xy}^s \delta k_{xy}^s + S_{yz}^s \delta \gamma_{yz}^s + S_{xz}^s \delta \gamma_{xz}^s\right] dA = 0
\end{aligned} \tag{14}$$

where A is the top surface and the stress resultants N, M, and S are defined by

$$\begin{Bmatrix} N_x & N_y & N_{xy} \\ M_x^b & M_y^b & M_{xy}^b \\ M_x^s & M_y^s & M_{xy}^s \end{Bmatrix} = \sum_{n=1}^{3} \int_{h_{n-1}}^{h_n} \left(\sigma_x, \sigma_y, \tau_{xy}\right)^{(n)} \begin{Bmatrix} 1 \\ z \\ f(z) \end{Bmatrix} dz \tag{15a}$$

$$\left(S_{xz}^s, S_{yz}^s\right) = \sum_{n=1}^{3} \int_{h_{n-1}}^{h_n} \left(\tau_{xz}, \tau_{yz}\right)^{(n)} g(z) dz \tag{15b}$$

where h_{n-1} and h_n are the top and bottom z-coordinates of the nth layer.

Substituting Eq. (10) into Eq. (15) and integrating through the thickness of the plate, the stress resultants are given as

$$\begin{Bmatrix} N \\ M^b \\ M^s \end{Bmatrix} = \begin{bmatrix} A & B & B^s \\ B & D & D^s \\ B^s & D^s & H^s \end{bmatrix} \begin{Bmatrix} \varepsilon \\ k^b \\ k^s \end{Bmatrix}, \qquad S = A^s \gamma \tag{16}$$

in which

$$N = \left\{N_x, N_y, N_{xy}\right\}^t, \qquad M^b = \left\{M_x^b, M_y^b, M_{xy}^b\right\}^t, \qquad M^s = \left\{M_x^s, M_y^s, M_{xy}^s\right\}^t, \tag{17a}$$

$$\varepsilon = \left\{\varepsilon_x^0, \varepsilon_y^0, \gamma_{xy}^0\right\}^t, \qquad k^b = \left\{k_x^b, k_y^b, k_{xy}^b\right\}^t, \qquad k^s = \left\{k_x^s, k_y^s, k_{xy}^s\right\}^t, \tag{17b}$$

$$A = \begin{bmatrix} A_{11} & A_{12} & 0 \\ A_{12} & A_{22} & 0 \\ 0 & 0 & A_{66} \end{bmatrix}, \quad A = \begin{bmatrix} B_{11} & B_{12} & 0 \\ B_{12} & B_{22} & 0 \\ 0 & 0 & B_{66} \end{bmatrix}, \quad D = \begin{bmatrix} D_{11} & D_{12} & 0 \\ D_{12} & D_{22} & 0 \\ 0 & 0 & D_{66} \end{bmatrix}, \tag{17c}$$

$$B^s = \begin{bmatrix} B_{11}^s & B_{12}^s & 0 \\ B_{12}^s & B_{22}^s & 0 \\ 0 & 0 & B_{66}^s \end{bmatrix}, \quad D^s = \begin{bmatrix} D_{11}^s & D_{12}^s & 0 \\ D_{12}^s & D_{22}^s & 0 \\ 0 & 0 & D_{66}^s \end{bmatrix}, \quad H^s = \begin{bmatrix} H_{11}^s & H_{12}^s & 0 \\ H_{12}^s & H_{22}^s & 0 \\ 0 & 0 & H_{66}^s \end{bmatrix}, \tag{17d}$$

$$S = \left\{S_{xz}^s, S_{yz}^s\right\}^t, \qquad \gamma = \left\{\gamma_{xz}, \gamma_{yz}\right\}^t, \qquad A^s = \begin{bmatrix} A_{44}^s & 0 \\ 0 & A_{55}^s \end{bmatrix}, \tag{17e}$$

and stiffness components are given as

$$\begin{Bmatrix} A_{11} & B_{11} & D_{11} & B_{11}^s & D_{11}^s & H_{11}^s \\ A_{12} & B_{12} & D_{12} & B_{12}^s & D_{12}^s & H_{12}^s \\ A_{66} & B_{66} & D_{66} & B_{66}^s & D_{66}^s & H_{66}^s \end{Bmatrix} = \int_{-h/2}^{h/2} Q_{11}(1, z, z^2, f(z), z\, f(z), f^2(z)) \begin{Bmatrix} 1 \\ \nu^{(n)} \\ \dfrac{1-\nu^{(n)}}{2} \end{Bmatrix} dz \tag{18a}$$

$$\left(A_{22}, B_{22}, D_{22}, B_{22}^s, D_{22}^s, H_{22}^s\right) = \left(A_{11}, B_{11}, D_{11}, B_{11}^s, D_{11}^s, H_{11}^s\right) \tag{18b}$$

$$A_{44}^{s} = A_{55}^{s} = \int_{-h/2}^{h/2} Q_{44}[g(z)]^2 dz, \tag{18c}$$

The variation of kinetic energy of the plate can be written as

$$\begin{aligned}
\delta T &= \int_{-\frac{h}{2}}^{\frac{h}{2}} \int_{\Omega} [\dot{u}\delta\,\dot{u} + \dot{v}\delta\,\dot{v} + \dot{w}\delta\,\dot{w}]\,\rho(z)\;dA\,dz \\
&= \int_{A} \{I_0[\dot{u}_0\delta\dot{u}_0 + \dot{v}_0\delta\dot{v}_0 + (\dot{w}_b + \dot{w}_s)(\delta\dot{w}_b + \delta\dot{w}_s)] \\
&\quad -I_1\left(\dot{u}_0\frac{\partial\delta\dot{w}_b}{\partial x} + \frac{\partial\dot{w}_b}{\partial x}\delta\,\dot{u}_0 + \dot{v}_0\frac{\partial\delta\dot{w}_b}{\partial y} + \frac{\partial\dot{w}_b}{\partial y}\delta\,\dot{v}_0\right) \\
&\quad -I_2\left(\dot{u}_0\frac{\partial\delta\dot{w}_s}{\partial x} + \frac{\partial\dot{w}_s}{\partial x}\delta\,\dot{u}_0 + \dot{v}_0\frac{\partial\delta\dot{w}_s}{\partial y} + \frac{\partial\dot{w}_s}{\partial y}\delta\,\dot{v}_0\right) \\
&\quad +J_1\left(\frac{\partial\dot{w}_b}{\partial x}\frac{\partial\delta\,\dot{w}_b}{\partial x} + \frac{\partial\dot{w}_b}{\partial y}\frac{\partial\delta\,\dot{w}_b}{\partial y}\right) + K_2\left(\frac{\partial\dot{w}_s}{\partial x}\frac{\partial\delta\,\dot{w}_s}{\partial x} + \frac{\partial\dot{w}_s}{\partial y}\frac{\partial\delta\,\dot{w}_s}{\partial y}\right) \\
&\quad +J_2\left(\frac{\partial\dot{w}_b}{\partial x}\frac{\partial\delta\,\dot{w}_s}{\partial x} + \frac{\partial\dot{w}_s}{\partial x}\frac{\partial\delta\,\dot{w}_b}{\partial x} + \frac{\partial\dot{w}_b}{\partial y}\frac{\partial\delta\,\dot{w}_s}{\partial y} + \frac{\partial\dot{w}_s}{\partial y}\frac{\partial\delta\,\dot{w}_b}{\partial y}\right)\Big\}\,dA
\end{aligned} \tag{19}$$

where dot-superscript convention indicates the differentiation with respect to the time variable t, $\rho(z)$ is the mass density, and (I_0, I_1, J_1, I_2, J_2, K_2) are mass inertias defined as

$$(I_0, I_1, J_1, I_2, J_2, K_2) = \sum_{n=1}^{3} \int_{h_{n-1}}^{h_n} (1, z, f, z^2, zf, f^2) dz \tag{20}$$

Substituting the expressions for δU and δT from equations (14), and (19) into equation (13) and integrating by parts, and collecting the coefficients of δu_0, δv_0, δw_b, and δw_s, the following equations of motion of the plate are obtained

$$\begin{aligned}
\delta\,u_0\text{:}\quad & \frac{\partial N_x}{\partial x} + \frac{\partial N_{xy}}{\partial y} = I_0\ddot{u}_0 - I_1\frac{\partial\ddot{w}_b}{\partial x} - J_1\frac{\partial\ddot{w}_s}{\partial x} \\
\delta\,v_0\text{:}\quad & \frac{\partial N_{xy}}{\partial x} + \frac{\partial N_y}{\partial y} = I_{01}\ddot{v}_0 - I_1\frac{\partial\ddot{w}_b}{\partial y} - J_1\frac{\partial\ddot{w}_s}{\partial y} \\
\delta\,w_b\text{:}\quad & \frac{\partial^2 M_x^b}{\partial x^2} + 2\frac{\partial^2 M_{xy}^b}{\partial x\partial y} + \frac{\partial^2 M_y^b}{\partial y^2} \\
& = I_0(\ddot{w}_b + \ddot{w}_s) + I_1\left(\frac{\partial\ddot{u}_0}{\partial x} + \frac{\partial\ddot{v}_0}{\partial y}\right) - I_2\nabla^2\ddot{w}_b - J_2\nabla^2\ddot{w}_s \\
\delta\,w_s\text{:}\quad & \frac{\partial^2 M_x^s}{\partial x^2} + 2\frac{\partial^2 M_{xy}^s}{\partial x\partial y} + \frac{\partial^2 M_y^s}{\partial y^2} + \frac{\partial S_{xz}^s}{\partial x} + \frac{\partial S_{yz}^s}{\partial y} \\
& = I_0(\ddot{w}_b + \ddot{w}_s) + J_1\left(\frac{\partial\ddot{u}_0}{\partial x} + \frac{\partial\ddot{v}_0}{\partial y}\right) - J_2\nabla^2\ddot{w}_b - K_2\nabla^2\ddot{w}_s
\end{aligned} \tag{21}$$

Introducing Eq. (16) into Eq. (21), the equations of motion can be expressed in terms of displacements (u_0, v_0, w_b, w_s) and the appropriate equations take the form

$$A_{11}\frac{\partial^2 u_0}{\partial x^2}+A_{66}\frac{\partial^2 u0}{\partial y^2}+(A_{12}+A_{66})\frac{\partial^2 v}{\partial x\partial y}-B_{11}\frac{\partial^3 w_b}{\partial x^3}-(B_{12}+2B_{66})\frac{\partial^3 w_b}{\partial x\partial y^2}$$
$$-B_{11}^s\frac{\partial^3 w_s}{\partial x^3}-(B_{12}^s+2B_{66}^s)\frac{\partial^3 w_s}{\partial x\partial y^2}=I_0\ddot{u}_0-I_1\frac{\partial\ddot{w}_b}{\partial x}-J_1\frac{\partial\ddot{w}_s}{\partial x}, \tag{22a}$$

$$(A_{12}+A_{66})\frac{\partial^2 u_0}{\partial x\partial y}+A_{66}\frac{\partial^2 v_0}{\partial x^2}+A_{22}\frac{\partial^2 v_0}{\partial y^2}-(B_{12}+2B_{66})\frac{\partial^3 w_b}{\partial x^2\partial y}-B_{22}\frac{\partial^3 w_b}{\partial y^3}$$
$$-B_{22}^s\frac{\partial^3 w_s}{\partial y^3}-(B_{12}^s+2B_{66}^s)\frac{\partial^3 w_s}{\partial x^2\partial y}=I_0\ddot{v}_0-I_1\frac{\partial\ddot{w}_b}{\partial y}-J_1\frac{\partial\ddot{w}_s}{\partial y} \tag{22b}$$

$$B_{11}\frac{\partial^3 u}{\partial x^3}+(B_{12}+2B_{66})\frac{\partial^3 u}{\partial x\partial y^2}+(B_{12}+2B_{66})\frac{\partial^3 v}{\partial x^2\partial y}+B_{22}\frac{\partial^3 v}{\partial y^3}-D_{11}\frac{\partial^4 w_b}{\partial x^4}$$
$$-2(D_{12}+2D_{66})\frac{\partial^4 w_b}{\partial x^2\partial y^2}-D_{22}\frac{\partial^4 w_b}{\partial y^4}-D_{11}^s\frac{\partial^4 w_s}{\partial x^4}-2(D_{12}^s+2D_{66}^s)\frac{\partial^4 w_s}{\partial x^2\partial y^2}-D_{22}^s\frac{\partial^4 w_s}{\partial y^4} \tag{22c}$$
$$=I_0(\ddot{w}_b+\ddot{w}_s)+I_1\left(\frac{\partial\ddot{u}_0}{\partial x}+\frac{\partial\ddot{v}_0}{\partial y}\right)-I_2\nabla^2\ddot{w}_b-J_2\nabla^2\ddot{w}_s,$$

$$B_{11}^s\frac{\partial^3 u}{\partial x^3}+(B_{12}^s+2B_{66}^s)\frac{\partial^3 u}{\partial x\partial y^2}+(B_{12}^s+2B_{66}^s)\frac{\partial^3 v}{\partial x^2\partial y}+B_{22}^s\frac{\partial^3 v}{\partial y^3}-D_{11}^s\frac{\partial^4 w_b}{\partial x^4}$$
$$-2(D_{12}^s+2D_{66}^s)\frac{\partial^4 w_b}{\partial x^2\partial y^2}-D_{22}^s\frac{\partial^4 w_b}{\partial y^4}-H_{11}^s\frac{\partial^4 w_s}{\partial x^4}-2(H_{12}^s+2H_{66}^s)\frac{\partial^4 w_s}{\partial x^2\partial y^2}-H_{22}^s\frac{\partial^4 w_s}{\partial y^4} \tag{22d}$$
$$+A_{55}^s\frac{\partial^2 w_s}{\partial x^2}+A_{44}^s\frac{\partial^2 w_s}{\partial y^2}=I_0(\ddot{w}_b+\ddot{w}_s)+J_1\left(\frac{\partial\ddot{u}_0}{\partial x}+\frac{\partial\ddot{v}_0}{\partial y}\right)-J_2\nabla^2\ddot{w}_b-K_2\nabla^2\ddot{w}_s$$

4.4 Exact solutions for P-FGMs sandwich plates

The exact solution of Eq. (22) for the P-FGMs sandwich plate under various boundary conditions can be constructed. The boundary conditions for an arbitrary edge with simply supported, clamped and free edge conditions are

- Simply supported (S)

$$N_x=v_0=w_b=w_s=M_x=0 \quad at \quad x=0,a \tag{23a}$$

$$N_y=u_0=w_b=w_s=M_y=0 \quad at \quad y=0,b \tag{23b}$$

- Clamped (C)

$$u_0=v_0=w_b=w_s=\frac{\partial w_b}{\partial x}=\frac{\partial w_s}{\partial x}=0 \quad at \quad x=0,a \tag{24a}$$

$$u_0=v_0=w_b=w_s=\frac{\partial w_b}{\partial y}=\frac{\partial w_s}{\partial y}=0 \quad at \quad y=0,b \tag{24b}$$

- Free (F)

Table 1 The admissible functions $X_m(x)$ and $Y_n(y)$

Boundary conditions					The functions $X_m(x)$ and $Y_n(y)$	
Notation	$x=0$	$y=0$	$x=a$	$y=b$	$X_m(x)$	$Y_n(y)$
SSSS	S	S	S	S	$sin(\lambda x)$	$sin(\mu x)$
CSCS	C	S	C	S	$sin^2(\lambda x)$	$sin(\mu x)$
CCCC	C	C	C	C	$sin^2(\lambda x)$	$sin^2(\mu x)$
FCFC	F	C	F	C	$cos^2(\lambda x)\,[sin^2(\lambda x)+1]$	$sin^2(\mu x)$

$$N_x = N_{xy} = \frac{\partial M_x}{\partial x} + 2\frac{\partial M_{xy}}{\partial y} = Q_x = M_x = 0 \quad at \quad x = 0, a \tag{25a}$$

$$N_{xy} = N_y + 2\frac{\partial M_{xy}}{\partial y} + \frac{\partial M_y}{\partial y} = Q_y = M_y = 0 \quad at \quad y = 0, b \tag{25b}$$

In the present problem, the following expressions are considered for the displacements that satisfy the considered boundary conditions

$$\begin{Bmatrix} u_0 \\ v_0 \\ w_b \\ w_s \end{Bmatrix} = \begin{Bmatrix} U_{mn}\dfrac{\partial X_m(x)}{\partial x}Y_n(y)e^{i\omega t} \\ V_{mn}X_n(x)\dfrac{\partial Y_n(y)}{\partial y}e^{i\omega t} \\ W_{bmn}X_n(x)Y_n(y)e^{i\omega t} \\ W_{smn}X_n(x)Y_n(y)e^{i\omega t} \end{Bmatrix} \tag{26}$$

where U_{mn}, V_{mn}, W_{bmn}, and W_{smn} are arbitrary parameters and $\omega = \omega_{mn}$ denotes the eigenfrequency associated with $(m,n)^{th}$ eigenmode. The functions $X_m(x)$ and $Y_n(y)$ are suggested by Sobhy (2013) to satisfy at least the geometric boundary conditions given in Eqs. (23), (24) and (25) and represent approximate shapes of the deflected surface of the plate. These functions, for the different cases of boundary conditions, are listed in Table 1 noting that $\lambda = m\pi/a$ and $\mu = n\pi/b$.

Substituting the Eq. (26) into the Eq. (22), and then multiplying each equation with the suitable eigenfunction and integrating over the domain of solution, after some mathematical rearraggement the following matrix format is gotten

$$\left(\begin{bmatrix} a_{11} & a_{12} & a_{13} & a_{14} \\ a_{12} & a_{22} & a_{23} & a_{24} \\ a_{13} & a_{23} & a_{33} & a_{34} \\ a_{14} & a_{24} & a_{34} & a_{44} \end{bmatrix} - \omega^2 \begin{bmatrix} m_{11} & 0 & m_{13} & m_{14} \\ 0 & m_{22} & m_{23} & m_{24} \\ m_{31} & m_{32} & m_{33} & m_{34} \\ m_{41} & m_{42} & m_{43} & m_{44} \end{bmatrix} \right) \begin{Bmatrix} U_{mn} \\ V_{mn} \\ W_{mn} \\ X_{mn} \end{Bmatrix} = \begin{Bmatrix} 0 \\ 0 \\ 0 \\ 0 \end{Bmatrix} \tag{27}$$

in which

$$\begin{aligned} a_{11} &= A_{11}\alpha_{12} + A_{66}\alpha_8 \\ a_{12} &= (A_{12} + A_{66})\alpha_8 \\ a_{13} &= -B_{11}\alpha_{12} - (B_{12} + 2B_{66})\alpha_8 \end{aligned} \tag{28}$$

$$
\begin{aligned}
a_{14} &= -(B_{12}^s + 2B_{66}^s)\alpha_8 - B_{11}^s\alpha_{12} \\
a_{21} &= (A_{12} + A_{66})\alpha_{10} \\
a_{22} &= A_{22}\alpha_4 + A_{66}\alpha_{10} \\
a_{23} &= -B_{22}\alpha_4 - (B_{12} + 2B_{66})\alpha_{10} \\
a_{24} &= -(B_{12}^s + 2B_{66})\alpha_{10} - B_{22}^s\alpha_4 \\
a_{31} &= B_{11}\alpha_{13} + (B_{12} + 2B_{66})\alpha_{11} \\
a_{32} &= (B_{12} + 2B_{66})\alpha_{11} + B_{22}\alpha_5 \\
a_{33} &= -D_{11}\alpha_{13} - 2(D_{12} + 2D_{66})\alpha_{11} - D_{22}\alpha_5 \\
a_{34} &= -D_{11}^s\alpha_{13} - 2(D_{12}^s + 2D_{66}^s)\alpha_{11} - D_{66}^s\alpha_5 \\
a_{41} &= B_{11}^s\alpha_{13} + (B_{12}^s + 2B_{66}^s)\alpha_{11} \\
a_{42} &= (B_{12}^s + 2B_{66}^s)\alpha_{11} + B_{22}^s\alpha_5 \\
a_{43} &= -D_{11}^s\alpha_{13} - 2(D_{12}^s + 2D_{66}^s)\alpha_{11} - D_{22}^s\alpha_5 \\
a_{44} &= -H_{11}^s\alpha_{13} - 2(H_{12}^s + 2H_{66}^s)\alpha_{11} - H_{22}^s\alpha_5 + A_{44}^s\alpha_9 + A_{55}^s\alpha_3
\end{aligned}
\tag{28}
$$

and

$$
\begin{aligned}
m_{11} &= -I_0\alpha_6 \qquad m_{13} = -I_1\alpha_6 \\
m_{32} &= -I_1\alpha_3 \qquad m_{14} = J_1\alpha_6 \\
m_{33} &= -I_0\alpha_1 + I_2(\alpha_3 + \alpha_9) \\
m_{22} &= -I_0\alpha_2 \qquad \text{and} \qquad m_{34} = -I_0\alpha_1 + J_2(\alpha_3 + \alpha_9) \\
m_{23} &= I_1\alpha_2 \qquad m_{41} = -J_1\alpha_9 \\
m_{24} &= J_1\alpha_2 \qquad m_{42} = -J_1\alpha_3 \\
m_{31} &= -I_1\alpha_9 \qquad m_{44} = -I_0\alpha_1 + K_2(\alpha_3 + \alpha_9)
\end{aligned}
\tag{29a}
$$

with

$$
\begin{aligned}
(\alpha_1, \alpha_3, \alpha_5) &= \int_0^b \int_0^a \left(X_m Y_n, X_m Y_n^{''}, X_m Y_n^{''''}\right) X_m Y_n dxdy \\
(\alpha_2, \alpha_4, \alpha_{10}) &= \int_0^b \int_0^a \left(X_m Y_n^{'}, X_m Y_n^{''}, X_m^{''} Y_n^{'}\right) X_m Y_n^{'} dxdy \\
(\alpha_6, \alpha_8, \alpha_{12}) &= \int_0^b \int_0^a \left(X_m^{'} Y_n, X_m^{'} Y_n^{''}, X_m^{'''} Y_n\right) X_m^{'} Y_n dxdy \\
(\alpha_7, \alpha_9, \alpha_{11}, \alpha_{13}) &= \int_0^b \int_0^a \left(X_m^{'} Y_n^{'}, X_m^{''} Y_n, X_m^{'} Y_n^{''}, X_m^{''''} Y_n\right) X_m Y_n dxdy
\end{aligned}
\tag{29b}
$$

The nontrivial solution is obtained when the determinant of Eq. (27) equals zero.

5. Numerical results and discussions

In this section, a series of numerical examples for free and vibration analysis of FG sandwich plates with porosity effects under general boundary conditions is presented and discussed.

Firstly, the validity, reliability and efficiency of the proposed solutions are verified by comparing the achieved numerical results with existing results in published literatures. Then, a parameter study regarding the effects of porosity parameters, porosity types, aspect ratio of the plates and boundary conditions is carried out systematically. The following five layer

configurations are used for multilayered P-FGM plates:

The (1-0-1) FGM sandwich plate: The plate is made of two layers of equal thickness without a core:

$$h_1 = h_3 = \frac{h}{2}, \qquad h_2 = 0$$

The (1-1-1) FGM sandwich plate: The plate is made of three equal-thickness layers:

$$h_1 = h_2 = h_3 = \frac{h}{3}$$

The (1-2-1) FGM sandwich plate: The core thickness equals the sum of faces thickness:

$$h_1 = h_3 = \frac{h}{4}, \qquad h_2 = \frac{h}{2}$$

The (2-1-2) FGM sandwich plate: The upper layer thickness is twice the core layer while it is the same as the lower one:

$$h_1 = h_3 = \frac{2h}{5}, \qquad h_2 = \frac{h}{5}$$

The (2-2-1) FGM sandwich plate: The core thickness is twice the upper face while it is the same as the lower one.

$$h_1 = h_2 = \frac{2h}{5}, \qquad h_3 = \frac{h}{5}.$$

The combination of materials consists of aluminum and alumina with the following material properties:

$$\text{Ceramic (alumina, } Al_2O_3\text{):} \quad E_c = 380\ GPa, \ \ \nu_c = 0.3, \ \ \rho_c = 3800\ kg/m^3.$$
$$\text{Metal (aluminum, Al):} \quad AE_m = 70\ GPa, \quad \nu_m = 0.3, \quad \rho_m = 2707\ kg/m^3.$$

The frequency parameter $\overline{\omega} = \frac{\omega a^2}{h}$ is used to express the non-dimensional frequency results of the sandwich plate.

5.1 Results verification

As the first example, the natural frequencies of FG sandwich square plate with SSSS boundary conditions versus different lay-up schemes and power-law index are tabulated in Table 2 and compared with the results of Zenkour (2005) based on sinusoidal shear deformation plate theory (SSDPT), trigonometric shear plate theory (TSDPT), Meksi *et al*. (2017) based on the hyperbolic shear deformation plate theory (HSDPT), and Li *et al*. (2008) based on the three-dimensional (3D) solutions. Good agreement is achieved between the present solution and the published ones. Besides, as the present theory includes only four unknowns in contrast to the five unknowns in the SSDPT and TSDPT make the present formulation more valuable.

Table 2 Dimensionless fundamental frequency of simply supported square power-law FGM sandwich plates ($a = 10h$)

k	Theory	Scheme				
		1-0-1	2-1-2	1-1-1	2-2-1	1-2-1
0	**Present**	**1.8245**	**1.8245**	**1.8245**	**1.8245**	**1.8245**
	3D (Li *et al*. 2008)	1.8268	1.8268	1.8268	1.8268	1.8268
	SSDPT (Zenkour 2005)	1.8245	1.8245	1.8245	1.8245	1.8245
	TSDPT (Zenkour 2005)	1.8245	1.8245	1.8245	1.8245	1.8245
	HSDPT (Meksi *et al*. 2017)	1.8257	1.8257	1.8257	1.8257	1.8257
0.5	**Present**	**1.4442**	**1.4841**	**1.5192**	**1.5471**	**1.5745**
	3D (Li 2008)	1.4461	1.4861	1.5213	1.5493	1.5767
	SSDPT (Zenkour 2005)	1.4444	1.4842	1.5193	1.5520	1.5745
	TSDPT (Zenkour 2005)	1.4442	1.4841	1.5192	1.5520	1.5727
	HSDPT (Meksi *et al*. 2017)	1.4448	1.4847	1.5199	1.5481	1.5756
1	**Present**	**1.2432**	**1.3001**	**1.3533**	**1.3957**	**1.4393**
	3D (Li 2008)	1.2447	1.3018	1.3552	1.3976	1.4414
	SSDPT (Zenkour 2005)	1.2434	1.3002	1.3534	1.4079	1.4393
	TSDPT (Zenkour 2005)	1.2432	1.3001	1.3533	1.4079	1.4393
	HSDPT (Meksi *et al*. 2017)	1.2432	1.3001	1.3533	1.4079	1.4393
5	**Present**	**0.9460**	**0.9818**	**1.0446**	**1.1089**	**1.1739**
	3D (Li 2008)	0.9448	0.9810	1.0453	1.1098	1.1757
	SSDPT (Zenkour 2005)	0.9463	0.9821	1.0448	1.1474	1.1740
	TSDPT (Zenkour 2005)	0.9460	0.9818	1.0447	1.1473	1.1740
	HSDPT (Meksi *et al*. 2017)	0.9455	0.9815	1.0446	1.1092	1.1744
10	**Present**	**0.9284**	**0.9429**	**0.9955**	**1.0610**	**1.1231**
	3D (Li 2008)	0.9273	0.9408	0.9952	1.0610	1.1247
	SSDPT (Zenkour 2005)	0.9288	0.9433	0.9952	1.0415	1.1346
	TSDPT (Zenkour 2005)	0.9284	0.9430	0.9955	1.1053	1.1231
	HSDPT (Meksi *et al*. 2017)	0.9279	0.9424	0.9952	1.0611	1.1234

5.2 Parametric studies

After verifying the accuracy of the present theory, parameter studies are carried out to investigate the influences of power law index k, thickness ratio of layers, i.e., scheme, boundary conditions, porosity parameters, and porosity types on natural frequency of FG sandwich plates.

Study 1:

The effects of power law index k and boundary conditions on the dimensionless fundamental frequencies of FG sandwich square plates are examined. The variations of the dimensionless fundamental frequencies of FG sandwich square plate versus different lay-up schemes and power-law index k are presented under different boundary conditions in Table 3 and Fig. 2. It is observed

Table 3 Effect of boundary conditions on dimensionless fundamental frequency of square power-law FGM sandwich plates ($a = 10h$)

Boundary conditions	k	Scheme				
		1-0-1	2-1-2	1-1-1	2-2-1	1-2-1
SSSS	0	1.8245	1.8245	1.8245	1.8245	1.8245
	0.5	1.4442	1.4841	1.5192	1.5471	1.5745
	1	1.2432	1.3001	13533	1.3957	1.4393
	5	0.9460	0.9818	1.0446	1.1089	1.1739
	10	0.9284	0.9429	0.9955	1.0610	1.1231
CSCS	0	2.6702	2.6702	2.6702	2.6702	2.6702
	0.5	2.1279	2.1863	2.2371	2.2768	2.3162
	1	1.8372	1.9212	1.9997	2.0594	2.1227
	5	1.4006	1.4575	1.5504	1.6440	1.7393
	10	1.3712	1.4000	1.4784	1.5739	1.6653
CCCC	0	3.2939	3.2939	3.2939	3.2939	3.2939
	0.5	2.6379	2.7100	2.7720	2.8200	2.8681
	1	2.2825	2.3870	2.4820	2.5560	2.6333
	5	1.7427	1.8170	1.9325	2.0474	2.1651
	10	1.7030	1.7456	1.8437	1.9611	2.0744
FCFC	0	3.4693	3.4693	3.4693	3.4693	3.4693
	0.5	2.7877	2.8637	2.9285	2.9783	3.0285
	1	2.4159	2.5263	2.6261	2.7032	2.7842
	5	1.8464	1.9278	2.0501	2.1706	2.2946
	10	1.8021	1.8522	1.9565	2.0799	2.1994

Table 4 The first five dimensionless frequencies of square plates ($a = 10h$, $k = 2$)

Scheme	Mode (m, n)	SSDPT (Zenkour 2005)	TSDPT (Zenkour 2005)	HPSDPT (Meksi *et al*. 2017)	Present
1-2-1	1 (1,1)	1.3024	1.3025	1.3032	**1.3024**
	2 (1,2)	3.1569	3.1570	3.1602	**3.1570**
	3 (2,2)	4.9085	4.9088	4.9161	**4.9092**
	4 (1,3)	6.0262	6.0267	6.0378	**6.0278**
	5 (2,3)	7.6360	7.6367	7.6556	**7.6402**
2-2-1	1 (1,1)	1.2678	1.2678	1 .2444	**1.2440**
	2 (1,2)	3.0738	3.0735	3.1094	**3.0177**
	3 (2,2)	4.7807	4.7800	4.6995	**4.6963**
	4 (1,3)	5.8702	5.8692	5.7739	**5.7692**
	5 (2,3)	7.4400	7.4385	7.3239	**7.3171**

that the hardest and softest plates correspond to the FCFC and SSSS ones, respectively (see Fig. 3). The effect of the power law index k on fundamental natural frequency of FG sandwich square plates is illustrated in Fig. 2. The thickness ratio of the plate is taken equal to 10. It can be seen that increasing the power law index k results in reduction of natural frequency (see Fig. 2). This is due to the fact that higher power law index k corresponds to lower volume fraction of the ceramic phase. In other word, increasing the power law index will reduce the stiffness of the plate due to high portion of metal in comparison with the ceramic part, and consequently, leads to a reduction of natural frequency.

Study 2:

To verify for higher-order modes, Table 4 shows the comparison of the first five natural frequencies of (1-2-1) and (2-2-1) FG sandwich plates. The thickness ratio a/h and power law index k of the plate are taken as 10 and 2, respectively. The obtained results are compared with those predicted by SSDT (Zenkour 2005), TSDT (Zenkour 2005) and HSDT (Meksi *et al*. 2017). A good agreement between the results is obtained for all vibration modes which confirm the accuracy of the present theory.

Study 3:

The influence of porosities distribution on the free vibration of P-FGM sandwich plates for side-to-thickness a/h = 10 and volume fraction index k = 1 is depicted in Table 5. The porosity coefficient is chosen as $\alpha = 0.1, 0.2$. It is clear that the frequency obtained for perfect plates $(\alpha = 0)$ is greater than that for $\alpha = 0.1$ and the latter is greater than that for $\alpha = 0.2$. In Fig. 4, the relationship between side-to-thickness (a/h) and fundamental frequency is presented for

Table 5 Effects of porosity on the dimensionless fundamental frequency of simply supported square power-law FGM sandwich plates (a = 10h, k = 1)

Sheme	Theories	Perfect	Imperfect I		Imperfect II		Imperfect III		Imperfect IV	
		$\alpha = 0$	$\alpha = 0.1$	$\alpha = 0.2$	$\alpha = 0.1$	$\alpha = 0.2$	$\alpha = 0.1$	$\alpha = 0.2$	$\alpha = 0.1$	$\alpha = 0.2$
	Present	**1.2432**	**1.1775**	**1.0990**	**1.2327**	**1.2209**	**1.2330**	**1.2221**	**1.2504**	**1.2584**
1-0-1	TSDPT	1.2432	1.1775	1.0990	1.2327	1.2209	1.2330	1.2221	1.2505	1.2585
	SSDPT	1.2434	1.1777	1.0992	1.2329	1.2212	1.2332	1.2223	1.2506	1.2586
	Present	**1.3533**	**1.2953**	**1.2297**	**1.3369**	**1.3191**	**1.3373**	**1.3208**	**1.3475**	**1.3412**
1-1-1	TSDPT	1.3533	1.2953	1.2297	1.3369	1.3191	1.3373	1.3208	1.3475	1.3413
	SSDPT	1.3534	1.2954	1.2298	1.3369	1.3192	1.3374	1.3209	1.3476	1.3414
	Present	**1.4393**	**1.3910**	**1.3379**	**1.4242**	**1.4081**	**1.4246**	**1.4096**	**1.4306**	**1.4213**
1-2-1	TSDPT	1.4393	1.3910	1.3379	1.4242	1.4081	1.4246	1.4096	1.4306	1.4213
	SSDPT	1.4393	1.3909	1.3379	1.4242	1.4081	1.4246	1.4096	1.4306	1.4213
	Present	**1.3001**	**1.2374**	**1.1648**	**1.2847**	**1.2678**	**1.2851**	**1.2694**	**1.2987**	**1.2972**
2-1-2	TSDPT	1.3001	1.2374	1.1649	1.2847	1.2678	1.2851	1.2694	1.2987	1.2972
	SSDPT	1.3002	1.2375	1.1649	1.2849	1.2679	1.2853	1.2696	1.2989	1.2974
	Present	**1.3957**	**1.3484**	**1.2942**	**1.3805**	**1.3641**	**1.3809**	**1.3657**	**1.3897**	**1.3833**
2-2-1	TSDPT	1.4069	1.3638	1.3149	1.3938	1.3796	1.3941	1.3809	1.4023	1.3973
	SSDPT	1.4070	1.3638	1.3149	1.3938	1.3797	1.3942	1.3810	1.4023	1.3973

different porosity models for scheme of layers (1-1-1) with $k = 1$ and $\alpha = 0.1$. It is seen from Fig. 4 that the results of frequencies increase with increasing of side-to-thickness ratio a/h. Also, the difference among the porosity models increases with increasing of a/h ratio. In higher values of a/h, the porosity distributions play important role on the free vibration behavior of sandwich FGM porous plates.

Fig. 5 show the effects of porosity coefficient (α) on the dimensionless fundamental frequencies for scheme of layer (1-1-1) for $k = 2$ and $a/h = 10$. As seen from Fig. 5, increasing the porosity coefficient (α) yields to increase the difference among of porosity models, significantly. The results of porosity model imperfect II and III are very close to each other.

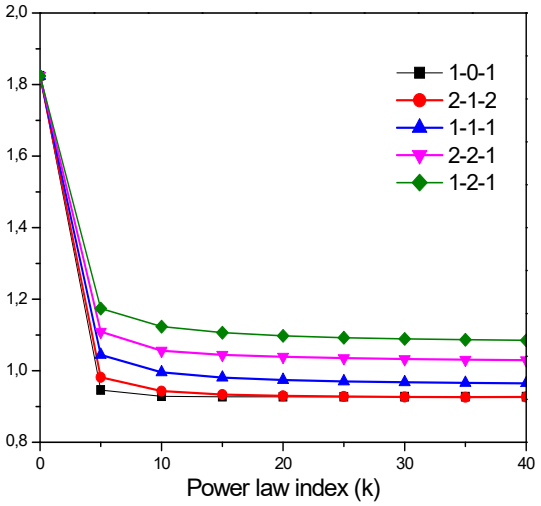

Fig. 2 Effect of power law index k on dimensionless fundamental frequency $\overline{\omega}$ of square plates ($a = 10h$)

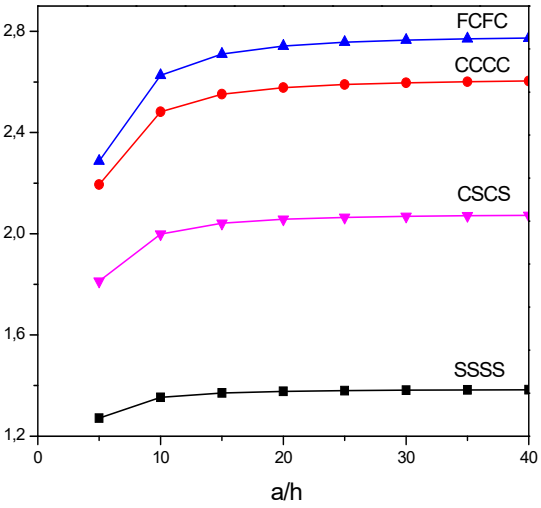

Fig. 3 Effect of boundary conditions on dimensionless fundamental frequency $\overline{\omega}$ of FG sandwich square plates ($k = 1$)

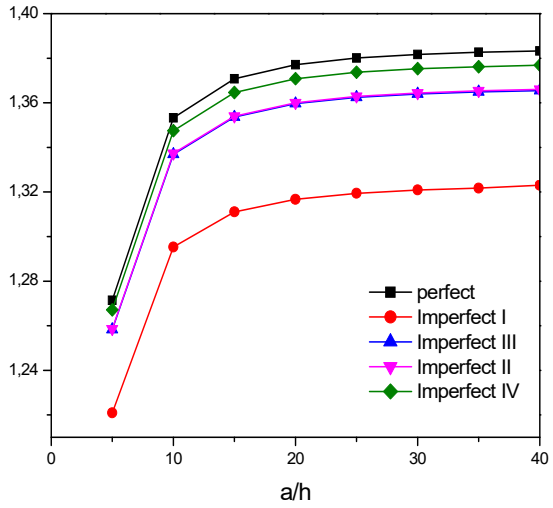

Fig. 4 Effect of side-to-thickness on dimensionless fundamental frequency $\overline{\omega}$ of perfect and porous FG sandwich square plate (1-1-1) (k = 1)

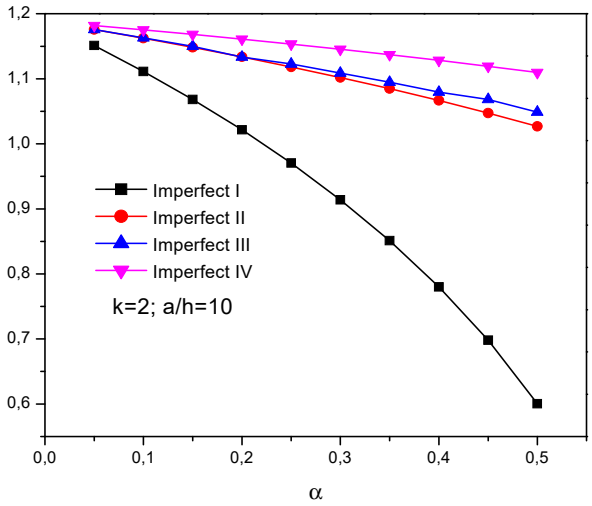

Fig. 5 Effect of porosity coefficient α on the dimensionless fundamental frequency $\overline{\omega}$ of FG sandwich square plate (1-1-1)

6. Conclusions

A simple refined shear deformation theory which eliminates the use of a shear correction factor was presented for FG sandwich plates composed of FG porous face sheets and an isotropic homogeneous core. Four models of porosity distribution are proposed. Governing equations and boundary conditions are derived from Hamilton's principle. Analytical solutions were obtained for free vibration analysis of square sandwich plates with FG porous layers under various boundary conditions. Several parametrical studies were performed for examining the effects of the porosity

volume fraction, type of porosity distribution model, side to thickness ratio, lay-up scheme, and boundary conditions on the free vibration of the FG sandwich plates.

Briefly, the following results were obtained:

- An excellent agreement can be seen between the current theory and previous theories.
- The values of the dimensionless fundamental frequency of FG sandwich plate decrease with the increase of the power-law index.
- The highest values of dimensionless fundamental frequencies of FG sandwich plates occur in FCFC boundary conditions while the lowest ones occur in SSSS boundary conditions.
- The side-to-thickness ration a/h has a significant influence on the free vibration frequencies, where the increasing of this geometrical parameter increases the non-dimensional frequencies.
- The non-dimensional frequencies are maximum for non-porous FG sandwich plates and decrease when the porosity coefficient increases regardless the porosity type.

Finally, it was concluded that the types of adopted porosity distribution model, porosity volume fraction, side to thickness ratio, lay-up scheme, and boundary conditions have significant effects on the free vibration of the FG sandwich plates.

References

Ahmadi, I. (2017), "A Galerkin layerwise formulation for three-dimensional stress analysis in long sandwich plates", *Steel Compos. Struct., Int. J.*, **24**(5), 523-536. https://doi.org/10.12989/scs.2017.24.5.523

Akbaş, Ş.D. (2017), "Vibration and static analysis of functionally graded porous plates", *J. Appl. Computat. Mech.*, **3**(3),199-207. https://doi.org/10.22055/JACM.2017.21540.1107

Ashoori, A.R., Vanini, S.A.S. and Salari, E. (2017), "Size-dependent axisymmetric vibration of functionally graded circular plates in bifurcation/limit point instability", *Appl. Phys. A*, **123**, 226. https://doi.org/10.1007/s00339-017-0825-5

Avcar, M. (2019), "Free vibration of imperfect sigmoid and power law functionally graded beams", *Steel Compos. Struct., Int. J.*, **30**(6), 603-615. https://doi.org/10.12989/scs.2019.30.6.603

Cuong-Le, T., Nguyen, K.D., Nguyen-Trong, N., Khatir, S., Nguyen-Xuan, H. and Abdel-Wahab, M. (2021), "A three-dimensional solution for free vibration and buckling of annular plate, conical, cylinder and cylindrical shell of FG porous-cellular materials using IGA", *Compos. Struct.*, **259**, 113216. https://doi.org/10.1016/j.compstruct.2020.113216

Daikh, A.A. and Zenkour, A.M. (2019), "Effect of porosity on the bending analysis of various functionally graded sandwich plates", *Mater. Res. Express*, **6**(6), 065703. https://doi.org/10.1088/2053-1591/ab0971

Delale, F. and Erdogan, F. (1983), "The crack problem for a nonhomogeneous plane", *J. Appl. Mech.*, **50**(6), 609-614. https://doi.org/10.1115/1.3167098

Ebrahimi, F. and Jafari, A. (2016), "A higher-order thermomechanical vibration analysis of temperature-dependent FGM beams with porosities", *J. Eng.*, **2016**. https://doi.org/10.1155/2016/9561504

Ebrahimi, F. and Salari, E. (2016), "Thermal loading effects on electro-mechanical vibration behavior of piezoelectrically actuated inhomogeneous size-dependent Timoshenko nanobeams", *Adv. Nano Res., Int. J.*, **4**(3), 197-228. https://doi.org/10.12989/anr.2016.4.3.197

Ebrahimi, F. and Salari, E. (2017), "Semi-analytical vibration analysis of functionally graded size-dependent nanobeams with various boundary conditions", *Smart Struct. Syst., Int. J.*, **19**(3), 243-257. https://doi.org/10.12989/sss.2017.19.3.243

Gupta, A. and Talha, M. (2018), "Influence of porosity on the flexural and free vibration responses of functionally graded plates in thermal environment", *Int. J. Struct. Stab. Dyn.*, **18**, 1850013.

https://doi.org/10.1142/S021945541850013X
Li, Q., Iu, V.P. and Kou, K.P. (2008), "Three-dimensional vibration analysis of functionally graded material sandwich plates", *J. Sound Vib.*, **311**(1-2), 498-515. https://doi.org/10.1016/j.jsv.2007.09.018
Meksi, R., Benyoucef, S., Mahmoudi, A., Tounsi, A., Adda Bedia, E.A. and Mahmoud, S.R. (2019), "An analytical solution for bending, buckling and vibration responses of FGM sandwich plates", *J. Sandw. Struct. Mater.*, **21**(2), 727-757. https://doi.org/10.1177/1099636217698443
Salari, E. and Vanini, S.A.S. (2021), "Investigation of thermal preloading and porosity effects on the nonlocal nonlinear instability of FG nanobeams with geometrical imperfection", *Eur. J. Mech.-A/Solids*, **86**, 104183. https://doi.org/10.1016/j.euromechsol.2020.104183
Salari, E., Ashoori, A. and Vanini, S.A.S. (2019), "Porosity-dependent asymmetric thermal buckling of inhomogeneous annular nanoplates resting on elastic substrate", *Adv. Nano Res., Int. J.*, **7**(1), 25-38. https://doi.org/10.12989/anr.2019.7.1.025
Salari, E., Vanini, S.A.S., Ashoori, A.R. and Akbarzadeh, A.H. (2020), "Nonlinear thermal behavior of shear deformable FG porous nanobeams with geometrical imperfection: Snap-through and postbuckling analysis", *Int. J. Mech. Sci.*, **178**, 105615. https://doi.org/10.1016/j.ijmecsci.2020.105615
Shahsavari, D., Shahsavari, M., Li, L. and Karami, B. (2018), "A novel quasi-3D hyperbolic theory for free vibration of FG plates with porosities resting on Winkler/Pasternak/Kerr foundation", *Aerosp. Sci. Technol.*, **72**, 134-149. https://doi.org/10.1016/j.ast.2017.11.004
Sobhy, M. (2013), "Buckling and free vibration of exponentially graded sandwich plates resting on elastic foundations under various boundary conditions", *Compos. Struct.*, **99**, 76-87. https://doi.org/10.1016/j.compstruct.2012.11.018
Taati, E. and Fallah, F. (2019), "Exact solution for frequency response of sandwich microbeams with functionally graded cores", *J. Vib. Control*, **25**(19-20), 2641-2655. https://doi.org/10.1177/1077546319864645
Wang, Z., Ruiken, A., Jacobs, F. and Ziegler, M. (2014), "A new suggestion for determining 2D porosities in DEM studies", *Geomech. Eng., Int. J.*, **7**(6), 665-678. https://doi.org/10.12989/gae.2014.7.6.665
Wattanasakulpong, N. and Ungbhakorn, V. (2014), "Linear and nonlinear vibration analysis of elastically restrained ends FGM beams with porosities", *Aerosp. Sci. Technol.*, **32**(1), 111-120. https://doi.org/10.1016/j.ast.2013.12.002
Wu, D., Liu, A., Huang, Y., Huang, Y., Pi, Y. and Gao, W. (2018), "Dynamic analysis of functionally graded porous structures through finite element analysis", *Eng. Struct.*, **165**, 287-301. https://doi.org/10.1016/j.engstruct.2018.03.023
Yang, J., Chen, D. and Kitipornchai, S. (2018), "Buckling and free vibration analyses of functionally graded graphene reinforced porous nanocomposite plates based on Chebyshev-Ritz method", *Composite Structures*, **193**, 281-294. https://doi.org/10.1016/j.compstruct.2018.03.090
Zenkour, A.M. (2005), "A comprehensive analysis of functionally graded sandwich plates: Part 2—Buckling and free vibration", *Int. J. Solids Struct.*, **42**, 5243-5258. https://doi.org/10.1016/j.ijsolstr.2005.02.016
Zouatnia, N., Hadji, L. and Kassoul, A. (2017), "An analytical solution for bending and vibration responses of functionally graded beams with porosities", *Wind Struct., Int. J.*, **25**(4), 329-342. https://doi.org/10.12989/was.2017.25.4.329

CC